Symmetry-Induced Error Filtering in a Photonic Lieb Lattice

Yi-Jun Chang, Yong-Heng Lu, Yao Wang, Xiao-Yun Xu, Wen-Hao Zhou, Wen-Hao Cui, Xiao-Wei Wang, Jun Gao, Lu-Feng Qiao, and Xian-Min Jin*

Center for Integrated Quantum Information Technologies (IQIT), School of Physics and Astronomy and State Key Laboratory of Advanced Optical Communication Systems and Networks, Shanghai Jiao Tong University, Shanghai 200240, China and

CAS Center for Excellence and Synergetic Innovation Center in Quantum Information and Quantum Physics, University of Science and Technology of China, Hefei, Anhui 230026, China

(Received 12 August 2020; accepted 26 January 2021; published 16 March 2021)

Quantum computation promises intrinsically parallel information processing capacity by harnessing the superposition and entanglement of quantum states. However, it is still challenging to realize universal quantum computation due that the reliability and scalability are limited by unavoidable noises on qubits. Nontrivial topological properties like quantum Hall phases are found capable of offering protection, but require stringent conditions of topological band gaps and broken time-reversal symmetry. Here, we propose and experimentally demonstrate a symmetry-induced error filtering scheme, showing a more general role of geometry in protection mechanism and applications. We encode qubits in a superposition of two spatial modes on a photonic Lieb lattice. The geometric symmetry endows the system with topological properties featuring a flat band touching, leading to distinctive transmission behaviors of π-phase qubits and 0-phase qubits. The geometry exhibits a significant effect on filtering phase errors, which also enables it to monitor phase deviations in real time. The symmetry-induced error filtering can be a key element for encoding and protecting quantum states, suggesting an emerging field of symmetry-protected universal quantum computation and noisy intermediate-scale quantum technologies.

DOI: 10.1103/PhysRevLett.126.110501

Quantum systems have been considered as powerful platforms for processing massive information and solving classically intractable problems by encoding qubits [1,2]. Analog quantum computation has demonstrated the supremacy over classical computation [3,4], whereas the step to universal quantum computation is still blocked by noises [5]. Fault tolerance is crucial for realizing reliable quantum computation, which has been explored on various systems, such as trapped ions [6], spins in semiconductors [7], superconducting circuits [8], solid state [9] and quantum optics [10]. However, implementation of error correction usually needs ancillary qubits with extra hardware overhead [11], which limits the scalability of quantum computation. For example, a qubit encoded in a superposition of two photonic modes may undergo phase errors in logical operations, which can be corrected by cluster states [12,13] but put daunting constraints for quantum systems including sources and measurements.

Geometries play a key role widely in natural and artificial materials, and induce extraordinary particle behaviors featured by localization and regular distribution [14–21]. Compared with dispersionless localization [22–24], the self-stabilization of distribution modes protected by geometries is more attractive for quantum computation, such as quantum Hall and anomalous quantum Hall phases with topological band gaps and broken time-reversal symmetry [25,26]. Regardless of the band topology, many symmetric geometries can equally create self-stabilizing states. Two-dimensional materials with rotational and inversion symmetries can bring about Dirac points possessing extraordinary properties of topological charges [27–29]. A Lieb lattice holds a square-hollow geometry with fourfold rotational symmetry [30–32], and builds a topological system with a flat band touching at Dirac points, which enables stable states with special phase features and makes it possible to implement a filter capable of exciting and stabilizing specific quantum states [33–35]. Such a filter will be able to eliminate phase errors and improve the purity of quantum states.

Our work is based on the photonic Lieb lattice with three sites forming a right triangle in each unit cell. Waveguides consisting of periodic unit cells are fabricated by femtosecond laser direct writing and are arranged in a ribbon, as shown in Fig. 1(a). The evolution of quantum states through the photonic lattice can be described by an equivalent Schrödinger equation $i\partial_z\Psi = \hat{H}\Psi$, with evolution length z considered as time t. The Hamiltonian is expressed by the tight-binding limit as [21],

$$\hat{H} = \sum_{\langle i,j \rangle} J a_i^\dagger a_j + \text{H.c.}, \tag{1}$$

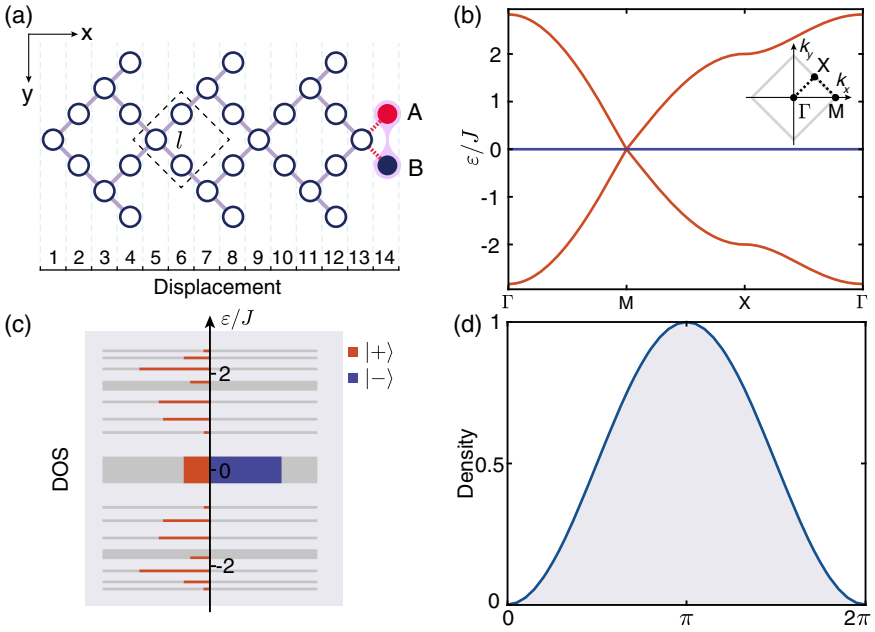

FIG. 1. Lieb lattice and energy spectrum. (a) Arrays of waveguides based on Lieb lattice. Dashed line frames out a unit cell and the nearest-neighbor spacing of lattice is l. Displacement along x axis of waveguides is in units of $l/\sqrt{2}$. Light is launched from two corner sites A and B at displacement 14. (b) Energy band of Lieb lattice in periodic boundary condition along a closed path in the momentum space. The path passes through three points, Γ, M, X, highlighted by dashed line in the first Brillouin zone of the inset. The red and blue lines suggest two dispersive bands and a flat band, respectively. (c) Eigenenergy spectrum of single-particle Hamiltonian and occupied DOS for input qubit Ψ_{in}. The thickness of rods indicates the number of degenerate modes. Qubit $|+\rangle$ (red) and qubit $|-\rangle$ (blue) correspond to 0-phase qubit and π-phase qubit, respectively. (d) Local density at displacement 14 of output Ψ_{out} as a function of phase ϕ.

where a_j and $a_i^\dagger$ are the annihilation and creation operators on sites j and i, respectively, and J is the hopping between nearest-neighbor sites.

In periodic boundary condition, the Lieb lattice holds three energy bands in momentum space. Because of four-fold rotational symmetry, the energy band holds three highly symmetric points in first Brillouin zone [36], as shown in Fig. 1(b). A flat band intersects the Dirac cones from dispersive bands, which leads to the real-space topology [37,38]. The density of states (DOS) at zero energy sharply increases and their group velocity is almost zero [18], which implies the emergence of localized states. By diagonalizing the matrix of $\hat{H}$, we acquire eigenenergy spectrum of our single-particle system [see Fig. 1(c)].

A qubit is launched to the lattice from two corner sites A and B at displacement 14, which is encoded as $\Psi_{\text{in}} = (|\varphi_A\rangle + e^{i\phi}|\varphi_B\rangle)/\sqrt{2}$, where $\varphi_{A(B)}$ denotes the basis wave function on site $A(B)$ and ϕ denotes the phase of mode on site B versus A. π-phase qubit ($\phi = \pi$) and 0-phase qubit ($\phi = 0$) correspond to $|-\rangle$ and $|+\rangle$ on the Bloch sphere [6], respectively. To precisely reveal evolution properties, we dissect the components of input qubits by calculating occupied DOS [39], defined by projecting the excited mode on eigenmodes, $\text{DOS} = |\langle\varphi_i|\Psi_{\text{in}}\rangle|^2, i = 1, \ldots, N$. $|+\rangle$ occupies distinct energies that lead to asynchronous overlay of eigenmodes and complete dissipation, whereas $|-\rangle$ is absolutely assembled of degenerate zero-energy modes, as shown in Fig. 1(c).

Local density at displacement 14 of Ψ_{out} that is tested at the stable region of propagation gradually decreases to zero as phase deviates away from π [see Fig. 1(d)]. Qubits drifting away from $\phi = \pi$ would be filtered out, and phase of qubits in the corner naturally stabilizes at π (see Supplemental Material, Sec. B [40]). We verify that local densities of Ψ_{out} are hardly affected by imperfections of qubits (see Supplemental Material, Sec. C for detailed analysis of intensity ratio [40]).

The experimental platform consists of measurement and manipulation on qubits, as shown in Fig. 2(a). Qubits are generated by an on-chip Mach-Zehnder interferometer (MZI) that is often used in gate operations [44], and two arms of MZI are heated by a gold resistor on the surface of photonic chip [see Fig. 2(b)]. Phase of qubits is dependent on the voltage across resistors due to thermal effect [45]. The MZIs and lattices are integrated together on a photonic chip, as shown in Fig. 2(a). To ensure sufficiently filtering out phase errors, we first need to verify the stable region by examining the samples of different evolution lengths without thermal phase shifters. After a rapid diffusion process, the local density at displacement 14 fluctuates around 0.5 as shown in Fig. 2(c) after the qubit $\Psi_{\text{in}}(\phi = \pi/2)$ is generated via a beam splitter of coupled waveguides [46]. With thermal phase shifters fixed, the lattice in this stable region can optimally distinguish qubits Ψ_{in} with different ϕ.

To experimentally verify the transmission of qubits, we inject heralded single photons generated from a

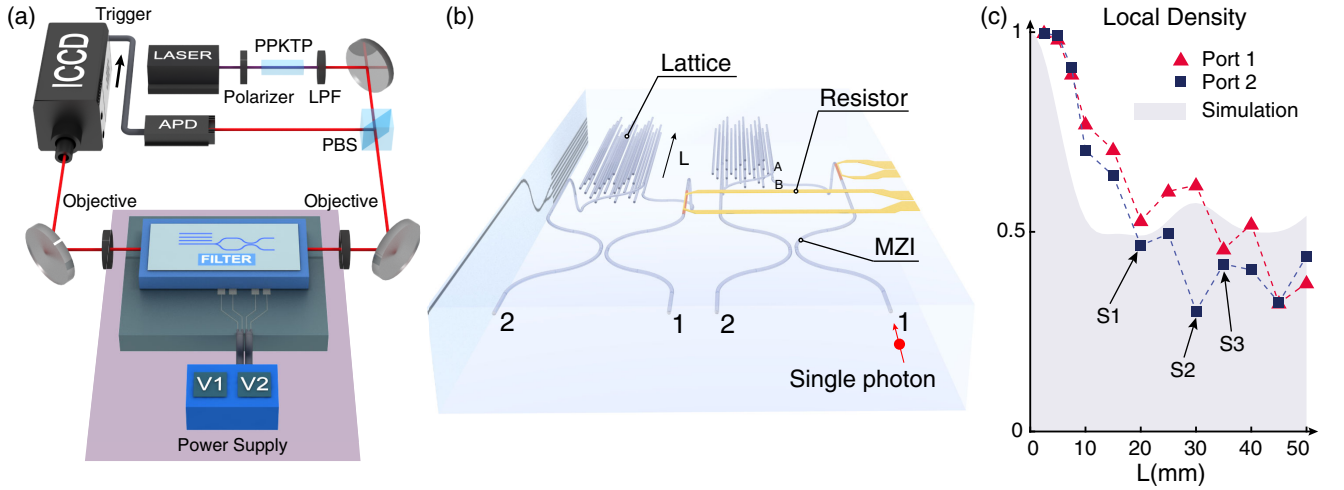

FIG. 2. Chip platform and propagation properties of lattices. (a) Control and measurement platform for chip. The photonic chip consists of Lieb lattices, MZIs and thermal phase shifters. External voltage signal is connected to manipulate phase of MZIs. Single photons generated from PPKTP crystals are used to examine the chip. LPF and PBS refer to long pass filter and polarization beam splitter, respectively. (b) Detailed structure of the photonic chip. The on-chip beam splitter separates the injected light into two channels, which are then connected to Lieb lattices with evolution length L. Parameters of waveguides are detailed in Supplemental Material, Sec. A [40]. Thermal phase shifters are connected to an external power supply that changes the current flowing through resistors. (c) Local density at displacement 14 of Ψ_{out} for different L. Results of tests are acquired by shooting the distribution of coherent light using charge-coupled device (CCD) camera. $\Psi_{\text{in}}(\phi = \pi/2)$ is generated without thermal phase shifter and local density at displacement 14 is basically stable at 0.5 from $L = 20$ mm. Samples with $L = 20$, 30, 35 mm, labeled by $S1$, $S2$, $S3$, respectively, are tuned by two integrated resistors.

periodically poled KTP (PPKTP) crystal into port 1 of the sample with $L = 20$ mm under modulation of on-chip MZIs [see Fig. 2(b)]. By imaging patterns with correlation measurement using intensified charge-coupled device (ICCD) camera (see Supplemental Material, Sec. F [40]), we obtain the probability distribution of photons with qubit information stored in phase.

After transferring on the lattice, qubits present significant difference in distributions with varying phase of Ψ_{in}. We quantify the transmission property of Ψ_{in} with the normalized probability, defined by using product transmission function [33],

$$T(\phi) = \left| \frac{\langle \varphi_A | \Psi_{\text{out}} \rangle \langle \varphi_B | \Psi_{\text{out}} \rangle}{\langle \varphi_A | \Psi_{\text{in}} \rangle \langle \varphi_B | \Psi_{\text{in}} \rangle} \right|^2. \tag{2}$$

As we can see in Fig. 3(a), transmission T is periodically related to ϕ varying quadratically with voltage V. Results denote that insertion loss is 4.3 dB for the central phase located at voltage $V_0 = 5.2$ V and that isolation can

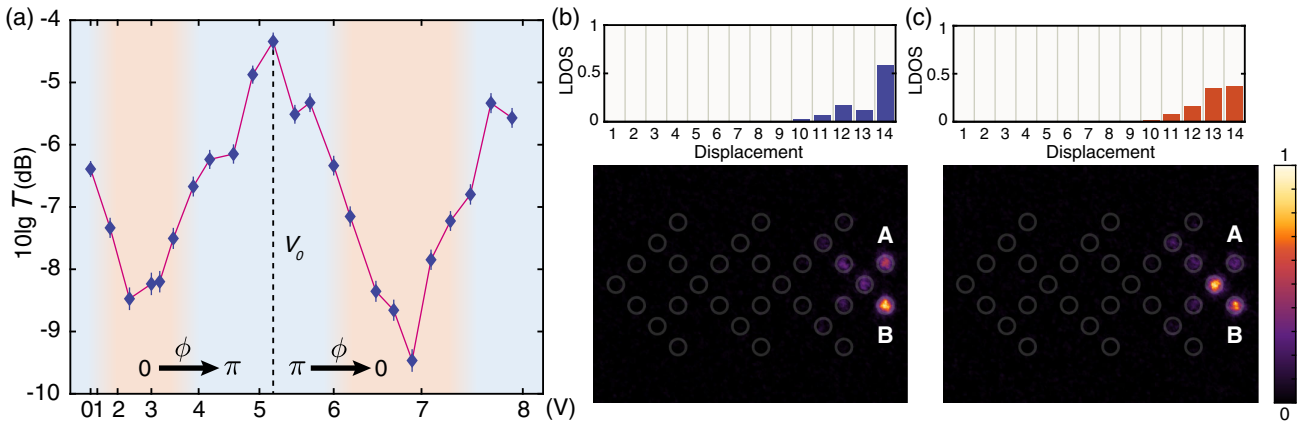

FIG. 3. Experimental results of symmetry-induced error filtering. (a) Transmission of Ψ_{in} with changing phase ϕ as a quadratic function of the voltage, see Supplemental Material, Sec. G for the definition of error bars [40]. A period of phase contains blue and red regions. One can infer that the phase of π (0) is located at the voltage of 5.2 (2.4 or 6.9) V. (b) and (c) display the local density of states (LDOS) of $\Psi_{\text{out}}(\phi = \pi)$ and $(\phi = 0)$, respectively, and the below are the corresponding experimental patterns.

reaches 5.1 dB between π and 0. The $|-\rangle$ state is preserved well at the initial position and $|+\rangle$ spreads into the bulk, as shown in Figs. 3(b) and 3(c). Qubits $|-\rangle$ and $|+\rangle$ are isolated both in phase space [8] and in real space so that they hardly overlap. The symmetric geometry realizes a nondestructive detection and filtering of phase deviations from $|-\rangle$ in real time.

We further notice that there exists a significant contrast between $|-\rangle$ and $|+\rangle$ in features of local density, as shown in Figs. 3(b) and 3(c). By establishing the visibility [47] of local density, $v = (D_{\text{corner}} - D_{\text{bulk}})/(D_{\text{corner}} + D_{\text{bulk}})$, where D_{corner} denotes the density at displacement $x = 14$ and D_{bulk} denotes the summed density between $x = 12 \sim 13$, we implement the function of recognizing encoded information in qubits without normalizing the LDOS. The visibilities for $\phi = \pi$ and $\phi = 0$ are 35.9% and -18.4%, respectively, which is able to discriminate the phase of Ψ_{in}.

To verify the feasibility and reliability of v for a phase discriminator, we examine the samples with three different evolution lengths by injecting coherent light into port 2 of them. The scope of visibilities in one cycle of phase and the LDOS of $\Psi_{\text{out}}(\phi = \pi/0)$ are shown in Figs. 4(a) and 4(b), respectively. We calibrate each sample by establishing a direct relationship between v of Ψ_{out} and ϕ of Ψ_{in}. For the three tested samples, the local density D_{corner} of $\Psi_{\text{out}}(\phi = \pi)$ exceeds D_{bulk} with visibility $v > 0$, whereas D_{corner} of $\Psi_{\text{out}}(\phi = 0)$ is weaker than D_{bulk} with $v < 0$. The gap between visibilities of π-phase and 0-phase qubits makes it success to quickly process the information encoded in qubits by only considering the local density.

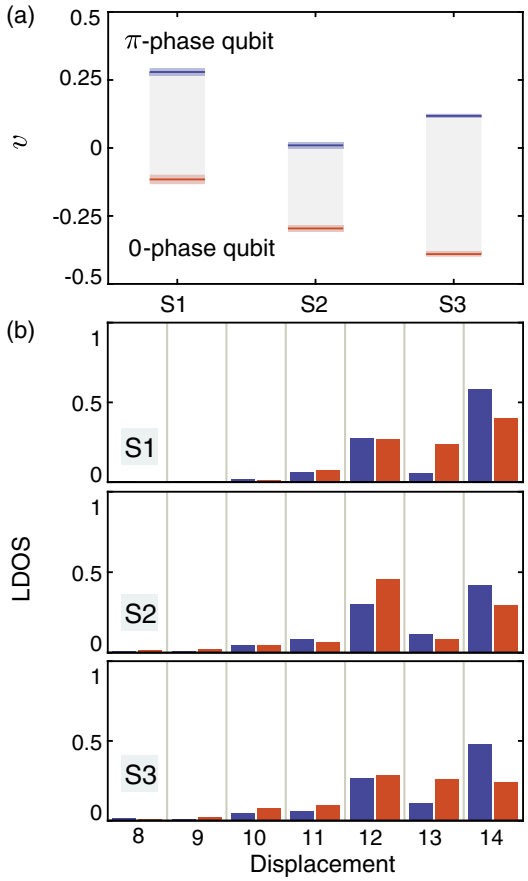

FIG. 4. Visibility v of local density for Ψ_{out}. (a) Scopes of v for three samples. Experimental samples, $S1$, $S2$, and $S3$, are labeled in Fig. 2(c). v for $\phi = \pi$ and $\phi = 0$ are highlighted in blue and red, respectively, and error bars of them are defined in Supplemental Material, Sec. G [40]. (b) LDOS of three samples, for $\phi = \pi$ and $\phi = 0$ (shown in blue and red, respectively).

In summary, we have successfully implemented a symmetry-induced error filtering for qubits by integrating the Lieb lattices, MZIs, and phase shifters on a single three-dimensional photonic chip. In our design, π-phase qubits are protected and qubits with phase deviations are filtered out spatially. We have also demonstrated controllable quantum information processing using three-dimensional circuits.

Our highly precise femtosecond laser direct writing technique makes it possible to explore the scalability of the symmetry-induced error filtering. The error filtering for various phase qubits and multiple qubits can also be realized based on the Lieb lattice (see Supplemental Material, Sec. L for details of scalability of the error filtering scheme [40]), which suggests an emerging field of symmetry-protected universal quantum computation. Furthermore, the symmetry-induced error filtering may be generalized to the qubits encoded in other degrees of freedom, such as vortex states [48,49], edge states with transverse momentum [50] in hexagonal lattices and two-photon states with bosonic and fermionic properties [51].

The authors thank Jian-Wei Pan for helpful discussions. This research is supported by the National Key R&D Program of China (No. 2019YFA0706302, No. 2019YFA0308700, No. 2017YFA0303700), the National Natural Science Foundation of China (No. 11904229, No. 11690033, No. 61734005, No. 11761141014), the Science and Technology Commission of Shanghai Municipality (STCSM) (No. 20JC1416300, No. 2019SHZDZX01, and No. 17JC1400403), and the Shanghai Municipal Education Commission (SMEC) (No. 2017-01-07-00-02-E00049). X.-M. J. acknowledges additional support from a Shanghai talent program and support from Zhiyuan Innovative Research Center of Shanghai Jiao Tong University.

*xianmin.jin@sjtu.edu.cn

[1] S. Lloyd, Universal quantum simulators, Science **273**, 1073 (1996).

[2] M. A. Nielsen and I. L. Chuang, *Quantum Computation and Quantum Information* (Cambridge University Press, Cambridge, England, 2010), p. 710.

[3] F. Arute *et al.*, Quantum supremacy using a programmable superconducting processor, Nature (London) **574**, 505 (2019).

[4] H. Wang *et al.*, Boson Sampling with 20 Input Photons and a 60-Mode Interferometer in a 10^{14}-Dimensional Hilbert Space, Phys. Rev. Lett. **123**, 250503 (2019).

[5] J. Preskill, Quantum computing in the NISQ era and beyond, Quantum **2**, 79 (2018).

[6] C. Flühmann, T. L. Nguyen, M. Marinelli, V. Negnevitsky, K. Mehta, and J. P. Home, Encoding a qubit in a trapped-ion mechanical oscillator, Nature (London) **566**, 513 (2019).

[7] T. F. Watson *et al.*, A programmable two-qubit quantum processor in silicon, Nature (London) **555**, 633 (2018).

[8] R. Lescanne, M. Villiers, T. Peronnin, A. Sarlette, M. Delbecq, B. Huard, T. Kontos, M. Mirrahimi, and Z. Leghtas, Exponential suppression of bit-flips in a qubit encoded in an oscillator, Nat. Phys. **16**, 509 (2020).

[9] C. Zu, W.-B. Wang, L. He, W.-G. Zhang, C.-Y. Dai, F. Wang, and L.-M. Duan, Experimental realization of universal geometric quantum gates with solid-state spins, Nature (London) **514**, 72 (2014).

[10] E. Knill, R. Laflamme, and G. J. Milburn, A scheme for efficient quantum computation with linear optics, Nature (London) **409**, 46 (2001).

[11] A. G. Fowler, M. Mariantoni, J. M. Martinis, and A. N. Cleland, Surface codes: Towards practical large-scale quantum computation, Phys. Rev. A **86**, 032324 (2012).

[12] J. L. O'Brien, A. Furusawa, and J. Vučković, Photonic quantum technologies, Nat. Photonics **3**, 687 (2009).

[13] C.-Y. Lu, W.-B. Gao, J. Zhang, X.-Q. Zhou, T. Yang, and J.-W. Pan, Experimental quantum coding against qubit loss error, Proc. Natl. Acad. Sci. U.S.A. **105**, 11050 (2008).

[14] S. Gopalakrishnan, J. C. Y. Teo, and T. L. Hughes, Disclination Classes, Fractional Excitations, and the Melting of Quantum Liquid Crystals, Phys. Rev. Lett. **111**, 025304 (2013).

[15] Q. Wang, H. Xue, B. Zhang, and Y. D. Chong, Observation of Protected Photonic Edge States Induced by Real-Space Topological Lattice Defects, Phys. Rev. Lett. **124**, 243602 (2020).

[16] S. M. Hashemi, U. Jagodič, M. R. Mozaffari, M. R. Ejtehadi, I. Muševič, and M. Ravnik, Fractal nematic colloids, Nat. Commun. **8**, 14026 (2017).

[17] X.-Y. Xu *et al.*, Shining light on quantum transport in fractal networks, arXiv:2005.13385.

[18] Y. Cao *et al.*, Correlated insulator behaviour at half-filling in magic-angle graphene superlattices, Nature (London) **556**, 80 (2018).

[19] P. Wang, Y. Zheng, X. Chen, C. Huang, Y. V. Kartashov, L. Torner, V. V. Konotop, and F. Ye, Localization and delocalization of light in photonic moiré lattices, Nature (London) **577**, 42 (2020).

[20] Y. Wang *et al.*, Observation of magic angle and wall state in twisted bilayer photonic graphene, arXiv:1911.09174.

[21] M. C. Rechtsman, J. M. Zeuner, A. Tünnermann, S. Nolte, M. Segev, and A. Szameit, Strain-induced pseudomagnetic field and photonic Landau levels in dielectric structures, Nat. Photonics **7**, 153 (2013).

[22] Y. Wang, Y.-H. Lu, J. Gao, K. Sun, Z.-Q. Jiao, H. Tang, and X.-M. Jin, Quantum topological boundary states in quasicrystals, Adv. Mater. **31**, 1905624 (2019).

[23] Y. Wang, X.-L. Pang, Y.-H. Lu, J. Gao, Y.-J. Chang, L.-F. Qiao, Z.-Q. Jiao, H. Tang, and X.-M. Jin, Topological protection of two-photon quantum correlation on a photonic chip, Optica **6**, 955 (2019).

[24] Y. Wang *et al.*, Topologically protected quantum entanglement, arXiv:1903.03015.

[25] S. Mittal, V. V. Orre, D. Leykam, Y. D. Chong, and M. Hafezi, Photonic Anomalous Quantum Hall Effect, Phys. Rev. Lett. **123**, 043201 (2019).

[26] C. Nayak, S. H. Simon, A. Stern, M. Freedman, and S. DasSarma, Non-Abelian anyons and topological quantum computation, Rev. Mod. Phys. **80**, 1083 (2008).

[27] M. Milićević, G. Montambaux, T. Ozawa, O. Jamadi, B. Real, I. Sagnes, A. Lemaître, L. Le Gratiet, A. Harouri, J. Bloch, and A. Amo, Type-III and Tilted Dirac Cones Emerging from Flat Bands in Photonic Orbital Graphene, Phys. Rev. X **9**, 031010 (2019).

[28] M. Milićević, T. Ozawa, G. Montambaux, I. Carusotto, E. Galopin, A. Lemaître, L. Le Gratiet, I. Sagnes, J. Bloch, and A. Amo, Orbital Edge States in a Photonic Honeycomb Lattice, Phys. Rev. Lett. **118**, 107403 (2017).

[29] Y.-H. Lu, Y. Wang, Y.-J. Chang, Z.-M. Li, W.-H. Cui, J. Gao, W.-H. Zhou, H. Zheng, and X.-M. Jin, Observing movement of Dirac cones from single-photon dynamics, Phys. Rev. B **103**, 064304 (2021).

[30] R. A. Vicencio, C. Cantillano, L. Morales-Inostroza, B. Real, C. Mejía-Cortés, S. Weimann, A. Szameit, and M. I. Molina, Observation of Localized States in Lieb Photonic Lattices, Phys. Rev. Lett. **114**, 245503 (2015).

[31] S. Xia *et al.*, Unconventional Flatband Line States in Photonic Lieb Lattices, Phys. Rev. Lett. **121**, 263902 (2018).

[32] W. Jiang, M. Kang, H. Huang, H. Xu, T. Low, and F. Liu, Topological band evolution between Lieb and kagome lattices, Phys. Rev. B **99**, 125131 (2019).

[33] B. Pal, Quasiperiodic magnetic chain as a spin filter for arbitrary spin states, Phys. Rev. B **99**, 134431 (2019).

[34] A. A. Kiselev and K. W. Kim, T-shaped ballistic spin filter, Appl. Phys. Lett. **78**, 775 (2001).

[35] I. A. Nechaev and E. E. Krasovskii, Spin filtering via resonant reflection of relativistic surface states, Phys. Rev. B **97**, 041407(R) (2018).

[36] M. R. Slot, T. S. Gardenier, P. H. Jacobse, G. C. P. van Miert, S. N. Kempkes, S. J. M. Zevenhuizen, C. Morais Smith, D. Vanmaekelbergh, and I. Swart, Experimental realization and characterization of an electronic Lieb lattice, Nat. Phys. **13**, 672 (2017).

[37] W.-F. Tsai, C. Fang, H. Yao, and J. Hu, Interaction-driven topological and nematic phases on the Lieb lattice, New J. Phys. **17**, 055016 (2015).

[38] R. Shen, L. B. Shao, B. Wang, and D. Y. Xing, Single Dirac cone with a flat band touching on line-centered-square optical lattices, Phys. Rev. B **81**, 041410(R) (2010).

[39] P. Umari, G. Stenuit, and S. Baroni, GW quasiparticle spectra from occupied states only, Phys. Rev. B **81**, 115104 (2010).

[40] See Supplementary Materials at http://link.aps.org/supplemental/10.1103/PhysRevLett.126.110501 for details, which includes Refs. [41–43].

[41] T. Li, P. Zhu, W. A. Benalcazar, and T. L. Hughes, Fractional disclination charge in two-dimensional C_n-symmetric topological crystalline insulators, Phys. Rev. B **101**, 115115 (2020).

[42] C. Li, W. Zhang, Y. V. Kartashov, D. V. Skryabin, and F. Ye, Bloch oscillations of topological edge modes, Phys. Rev. A **99**, 053814 (2019).

[43] Y. Wang *et al.*, Protecting quantum superposition and entanglement with photonic higher-order topological crystalline insulator, arXiv:2006.07963.

[44] A. Peruzzo, J. McClean, P. Shadbolt, M.-H. Yung, X.-Q. Zhou, P. J. Love, A. Aspuru-Guzik, and J. L. O'Brien, A variational eigenvalue solver on a photonic quantum processor, Nat. Commun. **5**, 4213 (2014).

[45] F. Flamini *et al.*, Thermally reconfigurable quantum photonic circuits at telecom wavelength by femtosecond laser micromachining, Light Sci. Appl. **4**, e354 (2015).

[46] A. Crespi, R. Osellame, R. Ramponi, D. J. Brod, E. F. Galvão, N. Spagnolo, C. Vitelli, E. Maiorino, P. Mataloni, and F. Sciarrino, Integrated multimode interferometers with arbitrary designs for photonic boson sampling, Nat. Photonics **7**, 545 (2013).

[47] P. Kok, W. J. Munro, K. Nemoto, T. C. Ralph, J. P. Dowling, and G. J. Milburn, Linear optical quantum computing with photonic qubits, Rev. Mod. Phys. **79**, 135 (2007).

[48] Y. Chen, J. Gao, Z.-Q. Jiao, K. Sun, W.-G. Shen, L.-F. Qiao, H. Tang, X.-F. Lin, and X.-M. Jin, Mapping Twisted Light into and out of a Photonic Chip, Phys. Rev. Lett. **121**, 233602 (2018).

[49] C. Jörg, G. Queraltó, M. Kremer, G. Pelegrí, J. Schulz, A. Szameit, G. von Freymann, J. Mompart, and V. Ahufinger, Artificial gauge field switching using orbital angular momentum modes in optical waveguides, Light Sci. Appl. **9**, 150 (2020).

[50] Y. Plotnik *et al.*, Observation of unconventional edge states in 'photonic graphene', Nat. Mater. **13**, 57 (2014).

[51] L. Sansoni, F. Sciarrino, G. Vallone, P. Mataloni, A. Crespi, R. Ramponi, and R. Osellame, Two-Particle Bosonic-Fermionic Quantum Walk via Integrated Photonics, Phys. Rev. Lett. **108**, 010502 (2012).